A Design for a Shock Ignition Experiment on the NIF Including 3-D Effects

Laura Tucker

Brighton High School

Rochester, New York

Advisor: Dr. R. S. Craxton

Laboratory for Laser Energetics

University of Rochester

Rochester, New York

January 2011

1. Abstract

A design for a plastic shell target has been developed for a proposed experiment for the National Ignition Facility (NIF) to investigate a two-stage shock-ignition concept in which 96 beams are used in each step (compression and ignition). To compensate for the NIF's beam configuration, the polar drive method was used, which involves pointing the beams toward the target equator. The beam pointings were also adjusted in the azimuthal direction. Two-dimensional hydrodynamic simulations using the code *SAGE* were combined with 3-D predictions of energy deposition to produce 3-D density profiles. Numerous simulations varying the selection of the 96 beams and the beam pointing, focusing, and energy ratios were used to identify an optimum design for the compression stage. Including variations in both θ and φ, the center of mass of the imploded shell has an rms deviation of just 8 μm after implosion through 400 μm.

2. Introduction

Nuclear fusion is a relatively recent approach to providing clean, renewable energy. One method used to achieve nuclear fusion is using laser beams to irradiate a target. The spherical target contains two hydrogen isotopes, deuterium and tritium, inside a shell of glass or plastic. When irradiated with the heat of the laser beams, the shell ablates outward and this force compresses the fuel inside the target thus creating a very high temperature and pressure environment. These extreme conditions compress the hydrogen isotopes, causing the nuclei to fuse and the fuel to explode. The deuterium and tritium fuse to form a helium nucleus and one energetic neutron. The remaining energy (that not collected from the released neutrons) is redeposited in a process known as ignition.

There are currently two different approaches to laser-driven nuclear fusion: direct drive and indirect drive. In direct drive fusion, laser beams hit the target at normal incidence from all directions [Figure 1(a)]. This is the type of fusion for which the beams of the University of Rochester's Laboratory for Laser Energetics' OMEGA laser system are configured. In indirect drive, the target sits inside a metal cylinder, usually made of gold, called a "hohlraum." Laser beams enter the hohlraum through openings in the top and bottom and penetrate the insides [Figure 1(b)]. Once hit by the beams, the walls of the hohlraum emit x rays which then irradiate the target and provide the energy needed for compression. Indirect drive implosions have the disadvantage of having much lower energy efficiency due to the fact that much of the laser energy is absorbed by the hohlraum or lost through the openings. Overall, only about 20% of the laser energy is actually absorbed by the target, but this lower efficiency is made up for by the greater uniformity of the x-ray radiation.

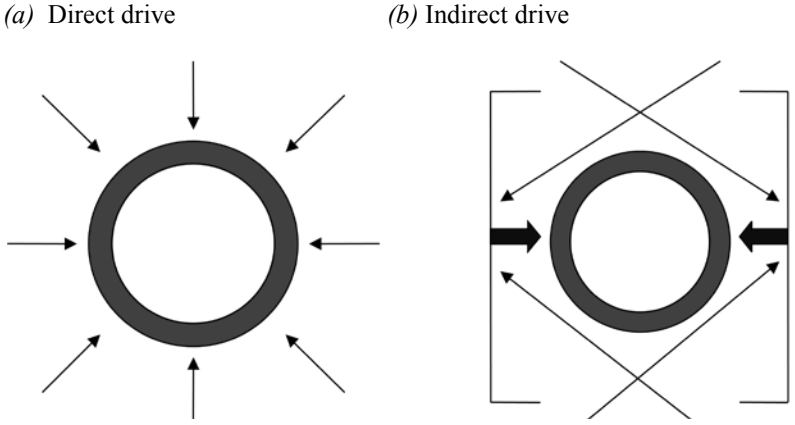

Figure 1. The two main approaches to inertial confinement fusion. (a) In direct drive, the laser beams directly irradiate the target. The thin lines represent these laser beams. (b) In indirect drive, the target is contained in a cylindrical hohlraum, which is hit on the insides by laser beams that enter through holes in the top and bottom. The hohlraum then produces x rays (represented by the thick lines) which irradiate the target.

The National Ignition Facility (NIF) at Lawrence Livermore National Laboratory is currently the world's largest and most powerful laser. Completed in 2009, the NIF beams are configured for indirect drive fusion experiments. The laser beam ports are arranged in four rings at angles θ of 23.5°, 30.0°, 44.5°, and 50.0° from the vertical in the upper hemisphere with four corresponding rings in the lower hemisphere. There are a total of 48 ports; laser beams are

arranged in groups of four called quads, so there is one quad per port. The fact that the beams are clustered near the poles is disadvantageous for direct drive fusion experiments. If the quads are simply pointed towards the center of the target, the equator will not be given as much drive as the poles and will therefore bulge as the target is compressed [Figure 2(a)]. This nonuniformity of implosion causes a severe loss of neutron production, which is not made up for even by the much greater energy of the NIF laser. Therefore, the beams of the laser must be repositioned away from the center of the target and towards the equator in a method called polar drive [Figure 2(b)].[1,2]

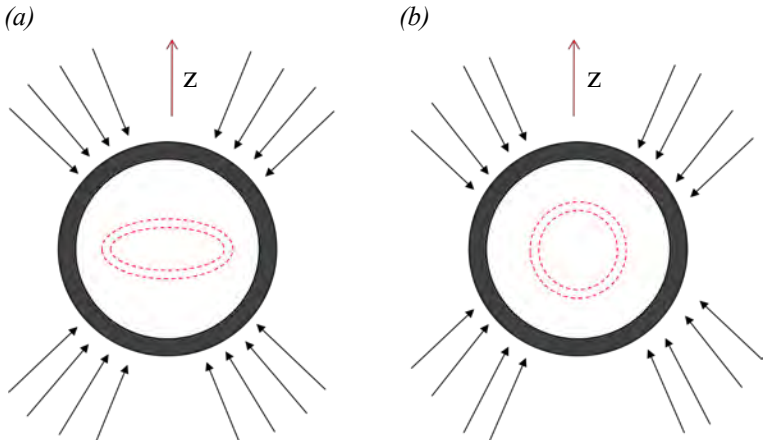

Figure 2. The possible NIF direct drive beam pointings and the resulting compression pattern of the target shell. (a) When the laser beams are pointed directly at the center of the target, the shell implodes nonuniformly. (b) By shifting the beams away from the target center and towards the equator, maximum implosion uniformity can be achieved.

3. Shock Ignition

Shock ignition[4] is a new concept for creating maximum-energy-gain fusion. Standard direct drive fusion experiments currently use a single long, high-intensity laser pulse which both compresses and ignites the target fuel in one step. A new proposal has recently been made to divide these laser pulses into two steps.[5] The first consists of a lower-intensity, longer laser pulse which is used to compress the target and bring the fuel as close together as possible without igniting it. The second pulse is called the shock pulse. It is extremely short and intense and its purpose is to create ignition. Due to design limitations, each NIF quad can only carry one type of pulse, and so the quads must be split between those used for the compression pulse and those

used for the shock pulse. For these designs, half of the quads were chosen to carry the compression pulse in a process that will be described in detail in this report, and the remaining quads were reserved for use in future experiments including the shock pulse [See Figure 3(a)]. The energy and duration of the initial and shock pulses compared to those of a conventional direct drive pulse can be seen in Figure 3(b).

(a) *(b)*

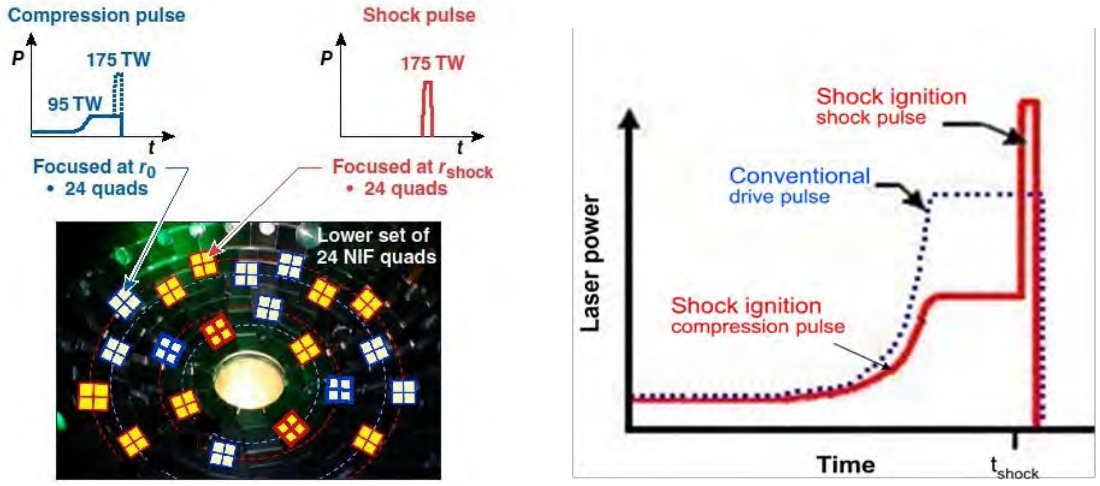

Figure 3. Graphical representations of conventional and shock ignition direct drive laser pulses. (a) Half of the NIF quads on both the top and bottom of the target chamber were chosen to be used in the compression pulse, therefore reserving the remaining quads for the shock pulse.[From Ref. 6] (b)The blue dotted line represents the conventional direct drive pulse, while the thick red line illustrates the initial compression pulse and the final, high-intensity shock pulse of shock ignition.

4. Shifting and Defocusing

The proposed shock ignition designs[6] use the method described in Refs. 7 and 8 to implement polar drive using existing NIF hardware. The key parameters available for creating these designs are the specifications for shifting the beam pointings in the vertical and horizontal directions, defocusing the beams, and choosing which quads to use in the compression pulse. Located near the end of the NIF laser system are mirrors (see Figure 4) which can be moved in order to shift the pointing of the individual beams (to an accuracy of about 50 microns in theory) and cause the center of the beam to hit the target at a different point on the surface. By

repositioning these beams, greater or less energy may be distributed to certain points on the target surface, and the shape of the imploding target may therefore be manipulated.

The defocus of the beams can be adjusted by repositioning the focus lens towards or away from the target. This causes the focal point of the laser beam to change and therefore the size and intensity of the beam spot to increase or decrease [see Figures 4(a) and (b)].

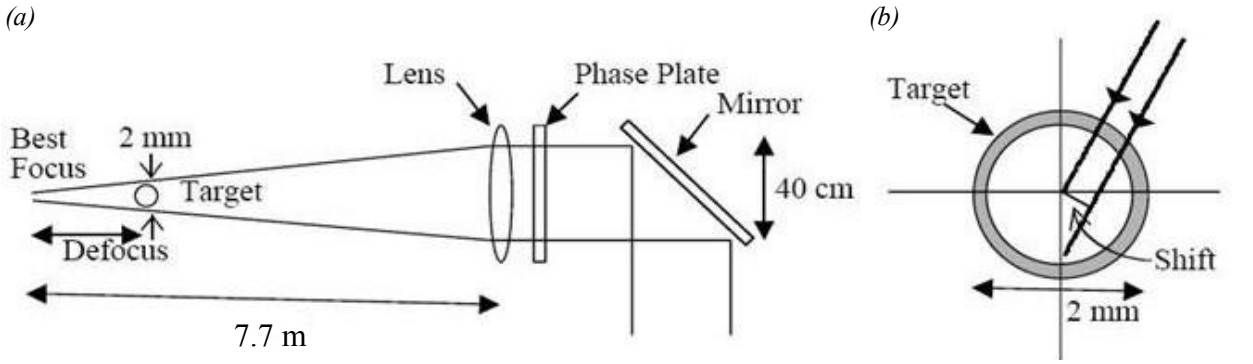

Figure 4. (a) Diagram (not to scale) showing the parts of the laser that control the parameters used in this work. Moving the lens along the beam axis controls the size of the beam at the target and tipping the mirror controls beam pointing. (b) Diagram showing how beam ring shifts are measured perpendicular to the beam direction. The angle of the beam from the vertical remains virtually constant. [From Ref. 7]

5. Optimization Process and the Optimized Designs

The goal of the optimization process was to develop a design, using only 24 of the NIF's 48 quads, that would cause the target shell to implode with maximum uniformity in both the azimuthal (Φ) and vertical (θ) directions. Several hundred 2-D hydrodynamic simulations including 3-D ray tracing were run using the code *SAGE* and analyzed, each with different variations of pointings, defocuses, and beam choices. The effects of certain variations were measured by isolating a single variable to be changed in increments and analyzing the outcomes of the changes. Initial analyses were based upon raytrace plots of target implosion and corresponding 1-D lineouts of average center-of-mass radius versus angle from the *z* axis (θ). Figure 5 shows two examples of the raytrace plots. Figure 5(a) depicts the target soon after the

laser pulse has been initiated and Figure 5(b) shows the target after it has imploded for 4 ns to a size of about half its original radius.

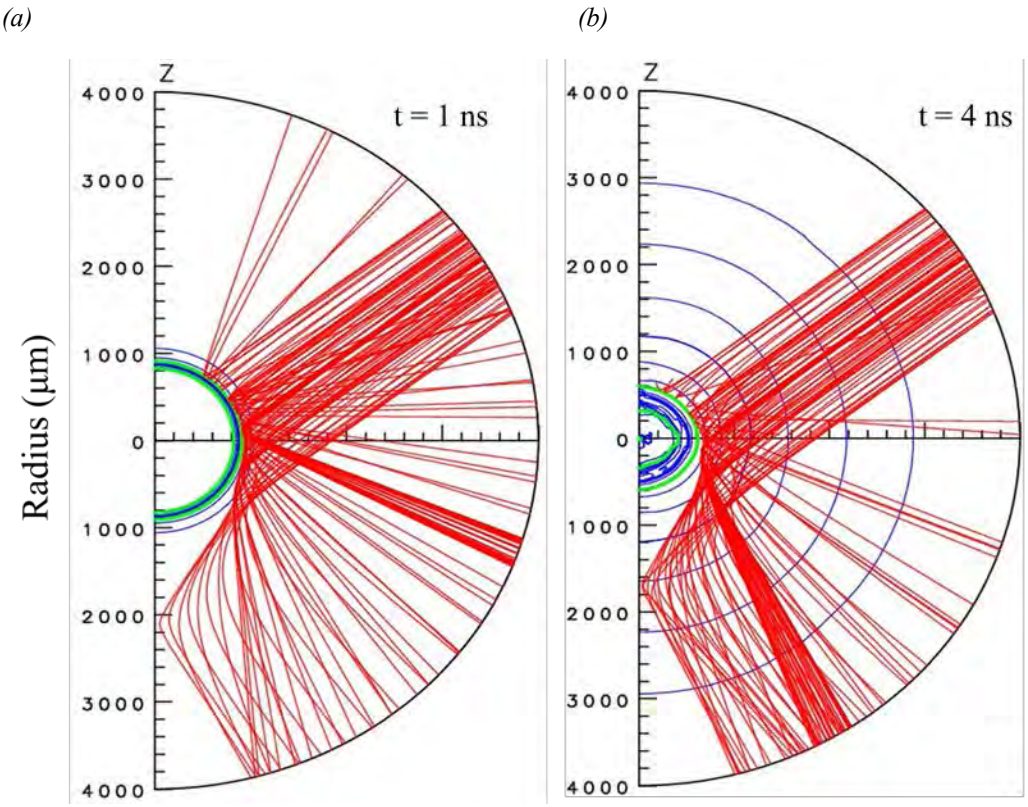

Figure 5. A comparison of two raytrace plots depicting the implosion of a target through time. (a) The relative position of the target shell is designated by the bright green lines. After only 1 ns of the laser being turned on, the shell has compressed inward very little from its original radius of 898 μm. (b) After 4 ns, which is the length of the entire compression pulse, the target shell has imploded to about half of its original radius. The red lines in each case represent the paths of the laser beams originating from the fourth ring of quads on the NIF- the row closest to the equator of the target chamber.

The importance of optimizing the design is shown in the differences between Figures 6(a) and 6(b). Figure 6(a) depicts the results of using an initial design reported in Ref. 9. The initial design shows the characteristic bulging at the equator (depicted by the bright green lines outlining the position of the target shell) that is common in polar drive designs for the NIF[10] due to the lack of drive at the equator. In the design with the optimized parameters, the bulge has been smoothed considerably. The beams pointed at the equator (the 50^{o} ring 4 of the NIF target

chamber) have also been given a tighter focus and 20% greater energy than the other beams in order to create greater intensity and therefore more equatorial drive.

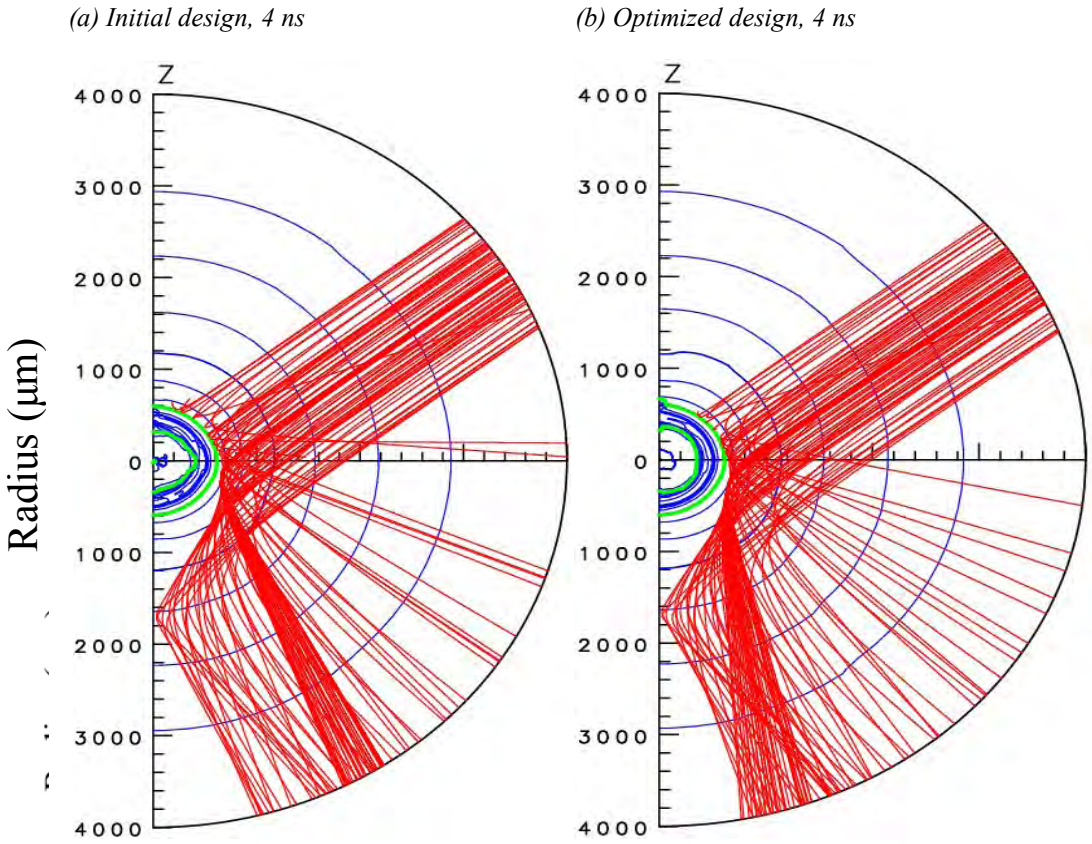

Figure 6. A comparison of two raytrace plots portraying the differences in the uniformity of the target compression after the laser beams have been on for 4 ns. (a) The initial design shows the protrusion at the equator that is common for targets compressed with polar drive on the NIF. (b) The optimized design limits the protrusion at the equator and greatly increases the circularity of the target.

These 2-D raytrace plots were converted into 1-D center-of-mass radius lineouts in order to better quantify the degree of nonuniformity in each of the target implosions. The radius of the target shell was plotted versus the vertical angle from the *z* axis for each case, and the root-mean-square deviation (rms) of the center-of-mass radius was calculated to determine the nonuniformity of the compression. The blue curve in Figure 7 depicts the target shell compression for the initial design, and can be compared with the red curve that depicts the

compression of the final, optimized design. As evidenced by the graph, the initial design has a much greater center-of-mass radius at the equator than elsewhere on the sphere, which means that the target shell is protruding in this region. The target shell in the optimized design has a much more even center-of-mass radius versus angle plot, meaning that the radius is similar throughout the shell and it is therefore a more spherical and uniform implosion.

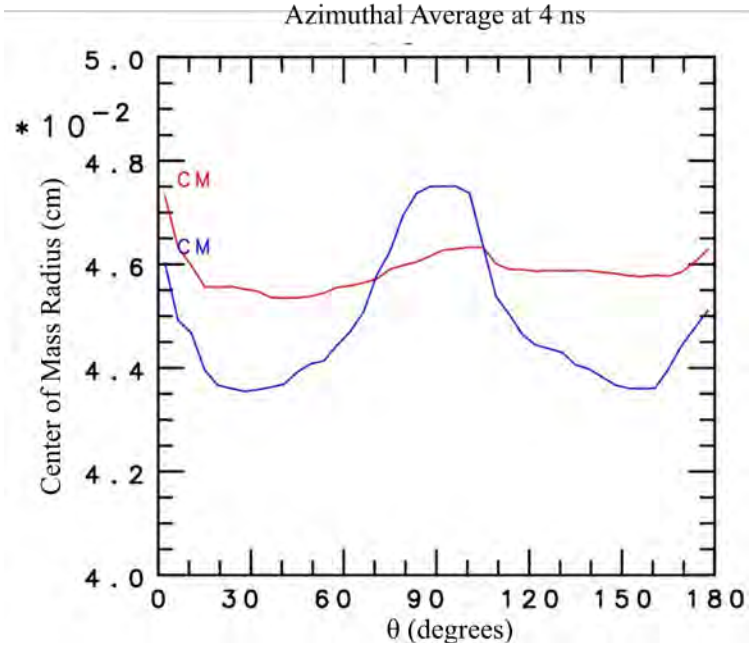

Figure 7. The center-of-mass radius plotted versus angle θ from the z axis for the initial and optimized designs. The lineout of the azimuthal average of the initial center-of-mass radius (blue) shows that the equator has not imploded as far as the poles and therefore needs extra drive to achieve even compression (rms = 3.10%). The lineout of the target shell in the optimized design (red) shows greatly improved implosion uniformity (rms = 0.64%).

The nonuniformity, measured by the rms of the center-of-mass radius, has been greatly reduced. At 4 ns, after the target shell has moved in approximately 450 μm from its original radius of 898 μm, the rms has changed from 3.10% (14.0 μm) in the original design to 0.64% (2.9 μm) in the optimized design. However, there are still some slight irregularities. A small protrusion still exists at the equator of the shell, as evidenced by the greater radius there. There are also peaks present at 0 and 180°, the poles of the target, which are caused by noise in the hydrodynamic simulation, as is the lack of symmetry in the graph. Without this noise, the target

nonuniformity would be even lower than 0.64%. The overall results of the optimized design are much smoother and have a much lower degree of nonuniformity than the initial design.

The next step of the optimization process was to maximize the azimuthal uniformity. Because only half of the NIF beams are used in the compression pulse, it cannot be assumed that the target will compress uniformly in the azimuthal direction. To estimate the three-dimensional uniformity, simulations were run that calculated the 3-D distribution of deposited energy on the surface of the target. To relate this quantity to the distance that the shell imploded, several hydrodynamic simulations were run, each with a differing amount of energy in the laser beams. By plotting the distance the shell imploded after 4 ns in each simulation versus the relative energy of the beams in that case, it was found that the increase in deposited energy is related to the increase in the distance moved inward by a factor of 0.72 (see Figure 8). This information was then used to create 3-D plots of the predicted center-of-mass radius.

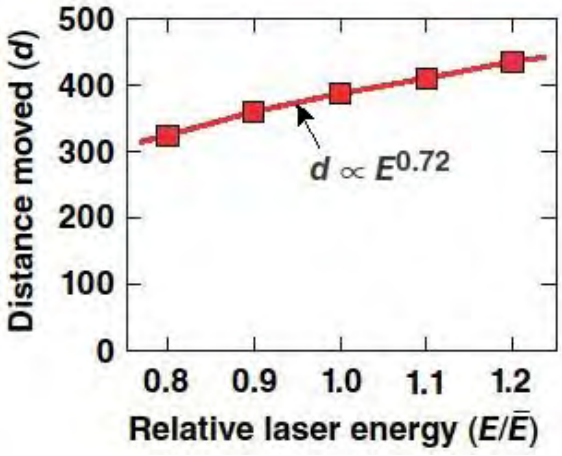

Figure 8. A graph plotting the distance the shell has imploded against the amount of energy in the laser beams. By observing the change in implosion distance versus the change in beam energy, it was found that the two were related by a factor of 0.72.

Figure 9 shows one such center-of-mass profile based on the initial design. The great variation in the radius can be seen from the large amplitudes of the peaks and valleys on the surface of the profile. The shaded-in quads represent those that are used for the laser pulse. The areas where the target is overcompressed (red) match these quads. In particular, the use of every

other quad in the first two rings results in a strong two-fold nonuniformity pattern around the azimuth near the poles.

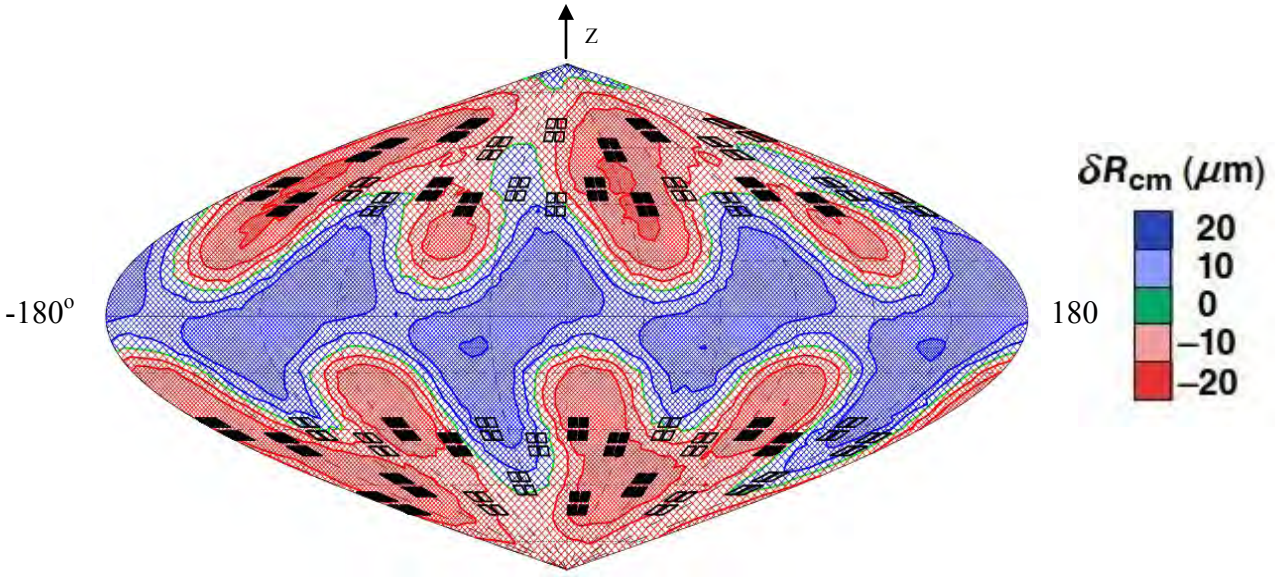

Figure 9. 3-D center-of-mass profile showing the azimuthal nonuniformity over the target surface at 4 ns in the initial design. The red represents the areas on the target shell that have a lower-than-average center-of-mass radius, and the blue illustrates the higher-than-average center-of-mass radii. The shaded-in quads represent the 24 which are used for the laser pulse. The target surface is not very evenly compressed, with a radius rms of 4.76% (21.7μm). This high degree of nonuniformity and the patterns in the center-of-mass radii are undesirable.

Variations in beam positioning, defocuses, and choices of beams used were tested until the optimal azimuthal uniformity was reached. For example, the bottom two beams in each quad in Ring 3 (known as Ring 3B) were given varying horizontal displacements in multiple simulations. These simulations were then analyzed in order to determine which displacement value would create the most uniform deposited energy profiles and therefore the most uniform target implosion (see Figure 10). In this case, we can see the distinct pattern of areas of high and low deposited energy when the beams were given very little horizontal displacement. As the beams moved more to the side, the pattern began to smooth out, providing a more even amount of energy to the target surface. Lastly, as the beams continued moving to the side, an inverted pattern appears from the beams overlapping again in different positions on the target shell.

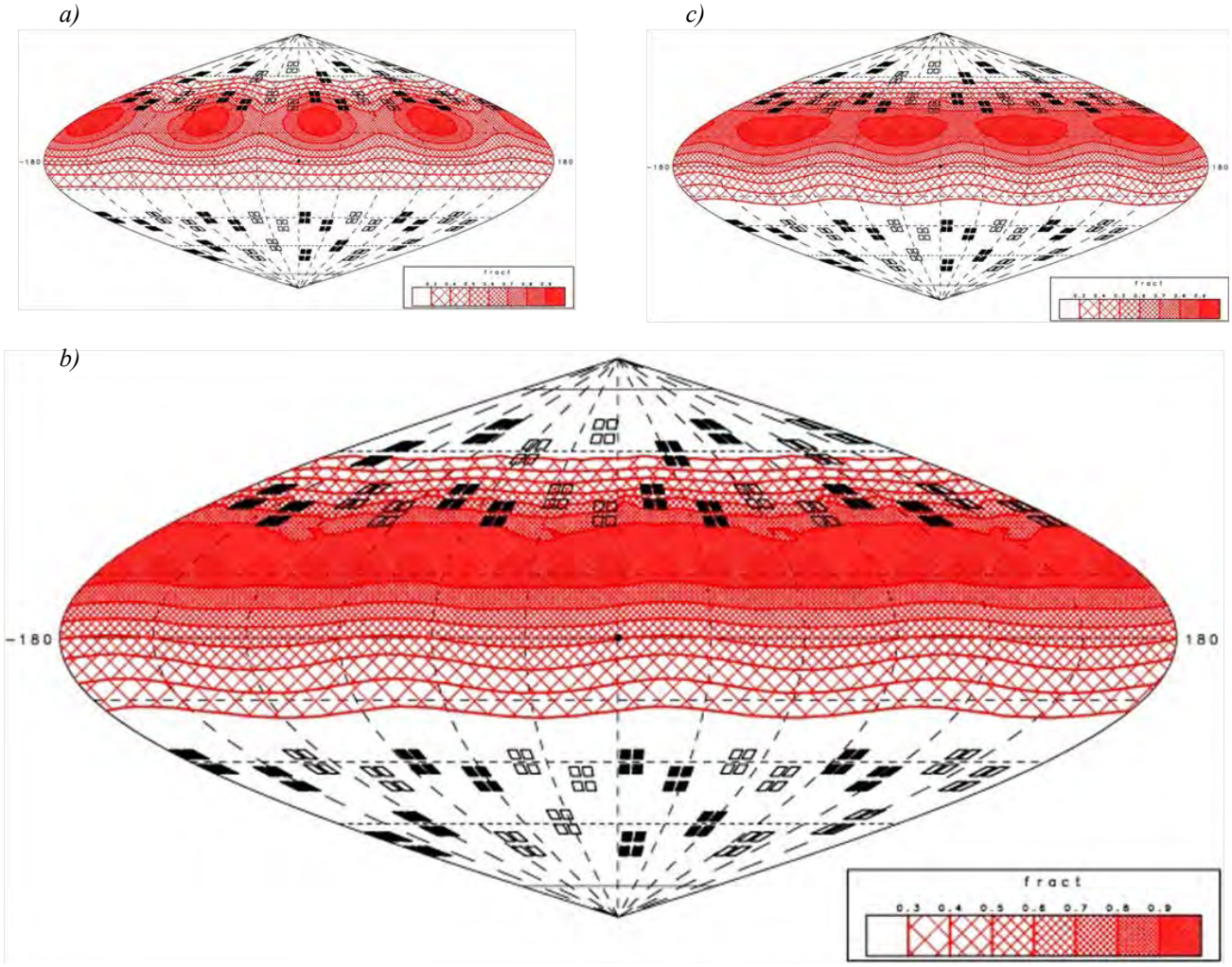

Figure 10. 3D cumulative deposited energy profiles at 4 ns for Ring 3B beams at various horizontal pointings Δy. The contours represent fractions of the maximum deposited energy, ranging from 0.3 to 0.9 with intervals of 0.1. (a) The horizontal pointings of the initial design (Δy=210 μm) caused very prominent patterns in the surface nonuniformity. (b) By adjusting the horizontal pointings, the deposited energy uniformity and therefore the center-of-mass radius uniformity were optimized (Δy=410 μm). (c) Shifting the beams too far in the horizontal direction caused an inversion in the cumulative deposited energy pattern (Δy=490 μm).

In attempts to achieve maximum azimuthal uniformity, the choice of quads used in the compression pulse was also altered from that of the original design. Since half of the beams were to be used in the compression stage, an alternating pattern of quads was chosen from each ring for the initial design, as shown in Figure 11(a). It was discovered during the optimization process that certain patterns in quad choice were more successful in providing uniform energy deposition

to the surface of the target shell. The final design continued to use alternating quads in Rings 3 and 4 but used all four quads in Ring 2 while using none of the quads in Ring 1 [Figure 11(b)].

(a) *(b)*

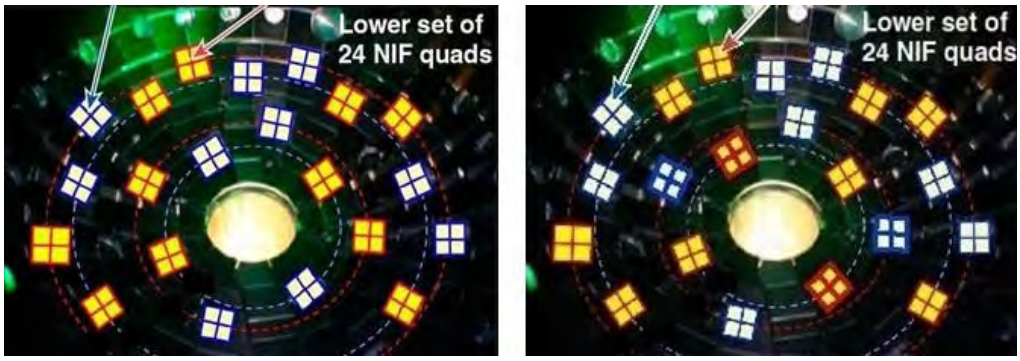

Figure 11. Images of the lower set of NIF quads depicting the quads used in each type of pulse in both the initial and optimized designs. (a) The initial design uses alternating quads from each ring to compress the target. The quads outlined in blue represent those used in the compression pulse stage. [From Ref. 5] (b) The optimized design uses all quads in Ring 2 and none of the quads in Ring 1 in the compression pulse in order to achieve optimal azimuthal implosion uniformity. [From Ref. 6]

The 3-D center-of-mass profile of the final design shows much greater uniformity of implosion (See Figure 12). The rms of the final design has been lowered by almost a factor of three to 1.76% (8.1 μm) after the target has moved in from 898 μm to 458 μm. The parameters of the final design are detailed in Table 1.

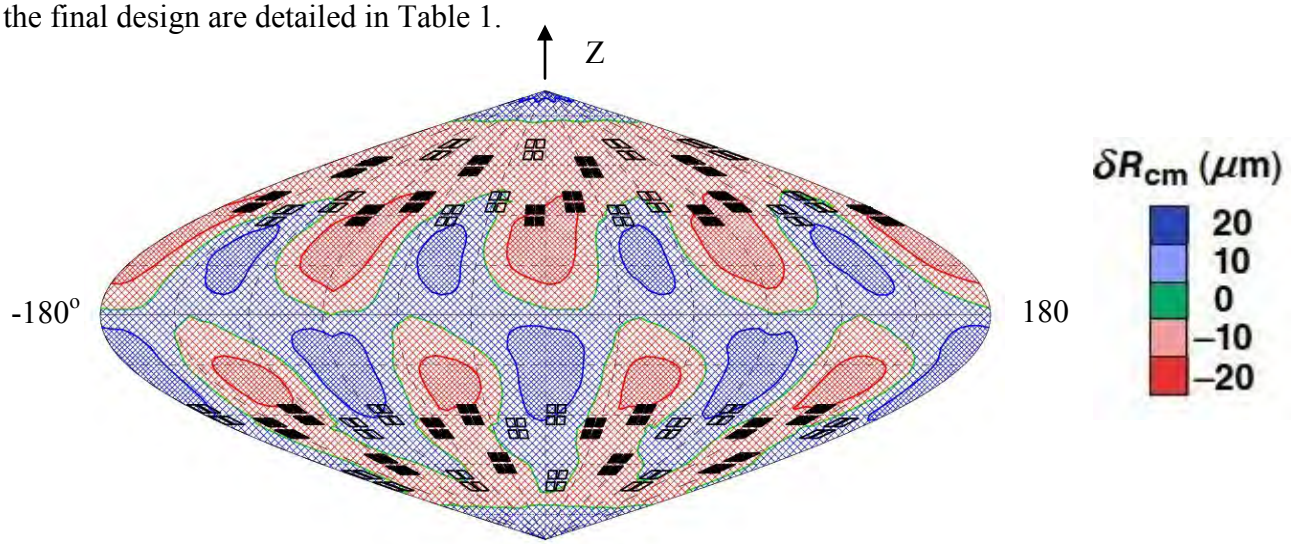

Figure 12. 3-D center-of-mass profile depicting azimuthal nonuniformity over the target surface at 4 ns in the final design. The nonuniformity of the center-of-mass radius has been greatly reduced over the azimuth, with an rms of 1.76% (8.1 μm) after moving inwards 440 μm.

Table 1. Beam parameter specifications (defocus and horizontal and vertical repointings) for the optimum design. The values of a and b indicate the half-intensity focal-spot radii of the phase plates currently installed on the NIF

Ring	θ	a, b (μm)	Defocus cm	Vert. PT (μm)	Horiz. PT (μm)
1A	21.24	882, 631	–	–	–
1B	25.93	882, 631	–	–	–
2A	28.01	824, 590	2.2	–70	0
2B	32.70	824, 590	2.2	–70	0
3A	42.19	635, 367	2.0	160	±250
3B	46.89	635, 367	1.7	–340	±380
4A	47.68	593, 343	1.2	–520	±420
4B	52.38	593, 343	1.0	–500	±450

6. Conclusion

An experimental design, taking into account beam defocus, beam choice, and pointing parameters, has been developed using 2-D hydrodynamic simulations with 3-D ray tracing to provide optimal implosion uniformity for proposed direct-drive shock ignition experiments on the NIF. Using the optimized design, it is possible to carry out shock ignition experiments on the NIF in the near future, using only 96 of the 192 total beams to compress the target shell. Specific beam pointings and defocuses have been chosen to provide optimal implosion uniformity.

7. Acknowledgments

I would like to sincerely thank Mr. Bradley Allen for encouraging me to participate in this program and my parents for furthering this encouragement. I would also like to thank my advisor Dr. R. Stephen Craxton for not only offering myself and many other students this incredible opportunity but also giving me invaluable guidance and support. Lastly, I am very grateful to the Laboratory for Laser Energetics for providing this program.

References

1. S. Skupsky, J. A. Marozas, R. S. Craxton, R. Betti, T. J. B. Collins, J. A. Delettrez, V. N. Goncharov, P. W. McKenty, P. B. Radha, T. R. Boehly, J. P. Knauer, F. J. Marshall, D. R. Harding, J. D. Kilkenny, D. D. Meyerhofer, T. C. Sangster, and R. L. McCrory, "Polar Direct Drive on the National Ignition Facility," Phys. Plasmas **11**, 2763 (2004).
2. R. S. Craxton, F. J. Marshall, M. J. Bonino, R. Epstein, P. W. McKenty, S. Skupsky, J. A. Delettrez, I. V. Igumenshchev, D. W. Jacobs-Perkins, J. P. Knauer, J. A. Marozas, P. B. Radha, and W. Seka, "Polar Direct Drive: Proof-of-Principle Experiments on OMEGA and Prospects for Ignition on the National Ignition Facility," Phys. Plasmas **12**, 056304 (2005).
3. R. Betti, C. D. Zhou, K. S. Anderson, L. J. Perkins, W. Theobald, and A. A. Solodov, "Shock Ignition of Thermonuclear Fuel with High Areal Density," Phys. Rev. Lett. **98**, 155001 (2007).
4. L. J. Perkins, R. Betti, K. N. LaFortune, and W. H. Williams, "Shock Ignition: A New Approach to High Gain Inertial Confinement Fusion on the National Ignition Facility," Phys. Rev. Lett. **103**, 045004 (2009).
5. L. J. Perkins *et al*., "Development of a Polar Drive Shock Ignition Platform on the National Ignition Facility," NIF Facility Time Proposal (2010).
6. R. S. Craxton, L. Tucker, T. Mo, K. S. Anderson. R. Betti, L. J. Perkins, G. P. Shurtz, X. Ribeyre, and A. Casner, "A 96/96-Beam Polar-Drive Configuration for Shock Ignition on the NIF," 52nd Annual Meeting of the American Physical Society, Division of Plasma Physics (2010).

7. Alexandra M. Cok, "Development of Polar Direct Drive Designs for Initial NIF Targets," Laboratory for Laser Energetics High School Summer Research Program (2006).
8. A. M. Cok, R. S. Craxton, and P. W. McKenty, "Polar-drive designs for optimizing neutron yields on the National Ignition Facility," Phys. Plasmas **15**, 082705 (2008).
9. R. S. Craxton, "2-D Polar-Drive Design for Shock Ignition on the NIF," Laboratory for Laser Energetics (April 2010), unpublished.
10. R. S. Craxton and D. W. Jacob-Perkins, "The Saturn Target for Polar Direct Drive on the National Ignition Facility," Phys. Rev. Lett. **94**, 095002 (2005).